

# A New Approach for In-situ Antenna Characterization, Radome Inspection and Radar Calibration, Using an Unmanned Aircraft System (UAS)

Simon Duthoit *Student, IEEE*, Jorge L. Salazar, *Senior, IEEE*  
William Doyle, Antonio Segales, Brent Wolf, Caleb. Fulton, *Senior, IEEE* and Phillip Chilson

**Abstract**—This paper presents a new concept for using an Unmanned Aircraft System (UAS) for in-situ antenna characterization, radome inspection and radar calibration. A commercial multirotor platform integrated with a sensor suite composed of an HD camera and an RF probe were used to prove the concept. Preliminary results were obtained using two different flight modes that were used to characterize an Antenna Under Test (AUT) and calibrate a radar in X-band. This new technique enables a full characterization of the antenna patterns in a radar system, including the external degradation introduced by factors such as ground clutter, the radome, temperature and other artifacts that are difficult to characterize during the design and development process. Preliminary results show that this technique has the potential for improving the characterization and the calibration process of an operational radar. This paper also presents a new UAS platform architecture that will be used for the same missions from S- to Ka-band in conventional and active phased array radar systems.

**Index Terms**—In-situ antenna measurements, UAV, UAS, DGPS, RTK, radar calibration, UAV antenna measurements, radome inspection.

## I. INTRODUCTION

Characterizing antenna patterns with high accuracy typically requires the use of specialized indoor or outdoor antenna range facilities. In both cases, the intrinsic properties of the antenna pattern measurements exclude the undesirable reflections, diffractions and other external sources of contamination that may influence the overall antenna performance. In a real situation the antenna interacts with external elements that can impact the antenna performance, depending on the application and site. In operational radar systems the antenna is mounted on a mechanical pedestal and is surrounded by other elements such as a radome, tower, lightning protection, and RF equipment. Ground irregularities produced by geography, morphology and environmental conditions (temperature and humidity) that are different for each site have been proven to negatively impact the overall performance of the radars, [1].

S. Duthoit, J. Salazar, W. Doyle, A. Segales, C. Fulton, B. Wolf are with the Department of Electrical and Computer Engineering and the Advanced Radar Research Center (ARRC) at the University of Oklahoma, Norman, OK, 73019 USA, see <http://www.arcc.ou.edu>, <http://www.ou-arcc-paard.com>.

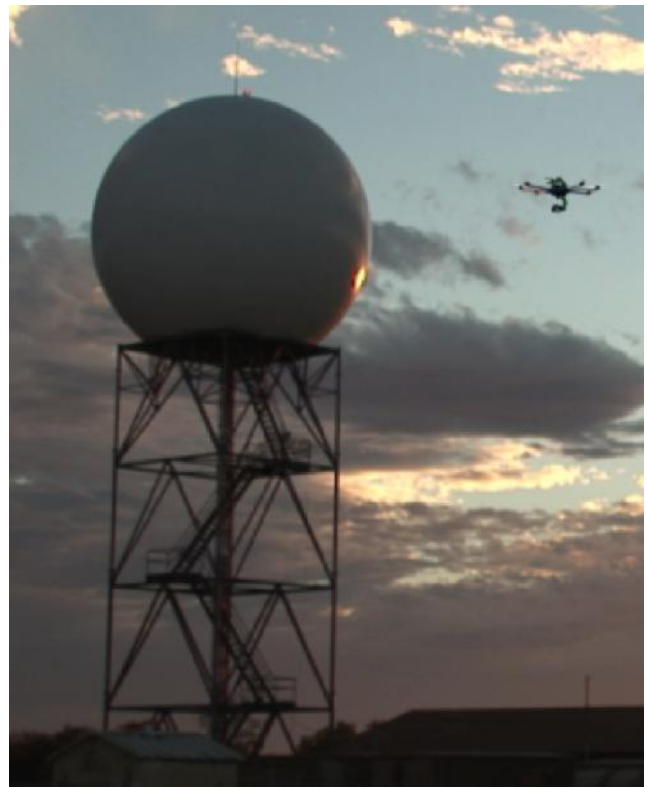


Fig. 1. Representation of in-situ antenna characterization, radome inspection and radar calibration using an Unmanned Aircraft System (UAS) for an operational NEXRAD radar system.

Dual-polarized radars require a high degree of matching (less than 0.1 dB) between the co-polar antenna radiation patterns for vertical and horizontal polarization [2]. A cross polarization isolation better than -25 dB is required for alternate transmit and alternate receive, and -40 dB is required for simultaneous transmit and receive in polarization mode [3]. Such cross polarization levels are possible to obtain in ideal conditions [4], [5], [6]. However, when antennas are exposed to a natural operational environment, the radiation patterns can be degraded [1], [7].

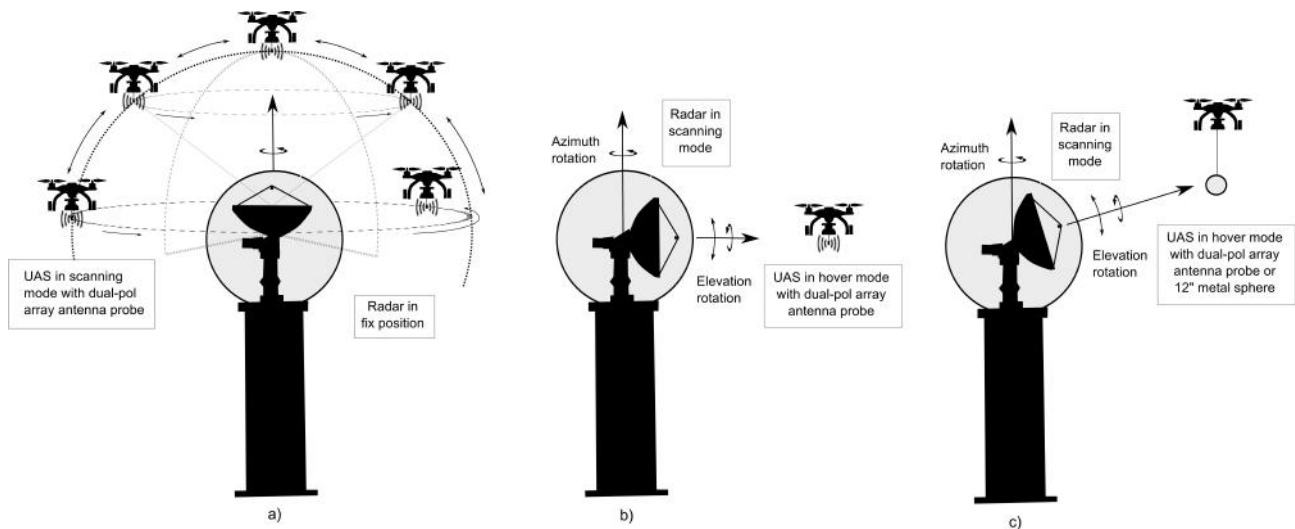


Fig. 2. Operation and scanning modes for antenna characterization and radar calibration. a) Full antenna or radar characterization when the UAS is in scanning mode. b) Antenna characterization for a single cut with the antenna rotating and the UAS in a fixed position (loitering). c) Radar calibration for reflectivity and differential reflectivity using a UAS in a fixed position (loitering).

Over the last eight years, several publications have reported measured results for manned and unmanned aircrafts. Using a helicopter, Manton in [1] characterized antenna patterns of a vertical array, including the effect of induced currents in the ground, and demonstrated how the antenna radiation patterns in elevation and azimuth are significantly affected by ground reflections. Current UAS technology has evolved significantly for the last five years. Today's UAS combine top quality gyro stabilization, inertial measurement units (IMU), and autonomous flight modes that allow vastly improved aerial stability, which in terms enables high quality 3-D maps, photogrammetry and lidar imagery. High performance flight controllers and a new generation of algorithms for differential GPS, such as Real Time Kinematics (RTK) algorithms, improved UAS positioning accuracy by two orders of magnitude (from 2-3 m to 1-4 cm) [8]. New adaptive controllers for multi-rotors allow very stable platforms that provide reliable operation in circumstances where the wind speeds are higher than 40 mph. New generation portable batteries and motors have improved the overall efficiency of the UAS and have extended its autonomy from standard durations of 15/20 min to more than 30 min. Recent publications show the results of in-situ antenna characterization using small UAS [9],[10],[11],[12], and [13].

As far as the radar calibration aspect goes, the differential reflectivity ( $Z_{dr}$ ) is a polarimetric variable of crucial importance, used for hydrometeor classification and weather data estimates such as rainfall rate for instance. Consequently a robust radar calibration method is needed to characterize and remove  $Z_{dr}$  bias in weather radar. The community has agreed on the 0.1 dB standard deviation value as being the 'Holy Grail' to aim for. No systematic method to consistently attain the latter goal has been devised so far. The most famous and used one remains the use of metal spheres tethered to helium balloons, as known


targets. Values as low as 0.2 dB have been obtained in [7]. In the summer of 2015, the UAV team of the Phased Array Antenna Research and Development group (PAARD) at the University of Oklahoma proposed the development of a UAS platform that would enable the aerial characterization of antennas, radome inspection and radar calibration. A few field experiments were carried out to prove the feasibility of both the antenna characterization and differential reflectivity radar calibration, using a commercial UAS platform (DJI Phantom 3). This paper presents, on top of preliminary results, the proposed concept of a UAS-based instrument for the missions stated.

## II. PROPOSED CONCEPT

The proposed concept consists of a platform capable of carrying a sensor suite that enables three important missions: a) in-situ antenna measurements, b) radome inspection, and c) radar calibration. To perform these missions, the UAS platform must be capable of supporting a payload of a few kilograms, in order to carry a 3-axis gimbal with a mounted RF probe consisting of an array antenna (it can be in S-, C- and X-bands) and a large bandwidth RF synthesizer, as well as HD optical and hyper-spectral cameras. The platform also requires additional sensors, such as lidar for high precision altimetry, and a DGPS system for sub-decimeter position accuracy. Large batteries ensure an operational endurance of up to 45 minutes, which is important for guaranteeing mission completion without interruptions.

### A. OU UAS' custom platform

The proposed platform is an octocopter built around a Tarot T18-1250 mm consumer frame. It uses 8 T-Motor U8 Pro motors that are waterproof and spin 18"x6" propellers. With two batteries the total weight is 16.5 kg. With four batteries it weighs 21.5 kg. The attendant flight times are 30 and 45



Features	Phantom 3	RD1000	OU- UAVRF1250
Flight time	20 min	20 min	30 -45min (2-4 batteries)
All-up weight	1.28 kg	2.15 kg	16.6 kg
Payload (after gimbal is mounted)	0 kg	0 kg	2200 gr
Size (diameter)	350 mm	550 mm	1250 mm
Propeller size	9 in x 5 in	9.4 in x 5 in	18 in x 6 in
Autopilot	DJI proprietary	RD100 Intelinair proprietary	Pixhawk autopilot
Trust efficiency	7 g/W-hour @ 50% Hover	7 g/W-hour @ 50% Hover	10 g/W-h @50% hover
Position accuracy	3-5 m (standard GPS)	3-5 m (standard GPS)	3-5 m (standard GPS) 2 -4 cm (D-GPS & RTK)
<b>Gimbal controller</b>	DJI proprietary	Feiyu tech mini 3d	Basecam
<b>Flight modes</b>	Manual / Loiter / Point of interest / User defined (in flight only) waypoints	Manual / Loiter / Any preflight defined waypoint mission	Manual / Loiter / Any preflight defined waypoint mission
DJI proprietary	DJI proprietary	Adaptive control	PID and Adaptive control

Fig. 3. UAS platforms and features comparison used for antenna characterization and radar calibration at the University of Oklahoma.

minutes respectively, depending on the number of batteries used. The onboard flight controller is the open source 3DR Pixhawk PX4. This controller enables automatic or manual flights (planned in a ground station) with or without the use of an eight-channel RC (radio controller). The GPS system was upgraded to DGPS using the RTK algorithm in order to improve the position accuracy (sub-decimeter). In addition, two IMUs (integrated within the Pixhawk) and a magnetometer (inside the GPS) assure the vehicle’s guidance. The platform also includes a lidar sensor to provide high precision altitude monitoring during landing and loitering. The 3D axis gimbal carries a 3 x 3 antenna array which is designed for low profile and low weight dual polarized performance. The UAS gimbal is designed to hold an antenna array for frequencies from S- to Ka-band. A picture of the proposed UAS is presented in Figure 4, alongside two commercial counterparts.

**B. Operation and scanning modes**

A UAS enables total scanning flexibility for in-situ antenna characterization and radar calibration. Figure 2 presents some of the modes that can be used. Figure 2 a) represents the mode when the antenna characterization and radar calibration can be performed with the antenna pointing in a fixed vertical position (at zenith). In this position, the antenna measurements are less contaminated by ground reflections. In this particular case, the flight of the UAS around the radar follows the spherical coordinate system. Figure 2 b) represents the mode when



Fig. 4. OU UAS’ platforms used for antenna characterization and radar calibration. On the left, the Intelinair RD100 platform with an X-band 4x4 dual polarized array antenna. In the middle, the OU UAVRF1250 with an S-band array of 3x3 elements. On the right, the Phantom 3 with a one-quarter-wavelength X-band monopole antenna

the UAS is loitering in a fixed position and the radar is in scanning mode. This mode can be used to quickly obtain a cut of the antenna patterns, or for performing reflectivity

(or differential reflectivity) calibration for different elevation angles. In addition, this mode enables the characterization of radar under the influence of clutter or ground reflections. Figure 2 c) represents the mode when the UAS is used for high performance radar calibration. In this case, the UAS is used to carry a metal sphere of 12 inches typically. The sphere is attached to the UAS far enough to separate the scattering of the UAS from the scattering of the sphere. 6-to-12-inch spheres attached to helium balloons have been used for calibration differential reflectivity. [7].

### III. PRELIMINARY RESULTS

Presented in this section are preliminary results of antenna characterization tests using a UAS (DJI Phantom 3). The tests were performed in both indoor and outdoor antenna range facilities. An X-band AUT was tested using a small monopole antenna (probe) attached to the frame of the UAS, since its gimbal cannot support any other additional payload than the mounted camera. An extra battery package was used to excite the RF synthesizer to transmit 24 dBm at 9.8 GHz. On the AUT side, a customized surface wave antenna is connected with an RF receiver, composed of LNAs, amplifiers and a power spectrum analyzer, to compensate for losses in the air and cables. The AUT rotates on a turntable in azimuth, which means the 0-degree elevation angle azimuthal cut of the radiation pattern is measured. The measurement procedure is fully automated by a Labview program that controls the turntable as well as the power spectrum analyzer. Figure 5 (top) and Figure 6a show the setup for indoor and outdoor measurements.

#### A. Antenna measurements

1) *Indoor measurements:* This part aims at characterizing the AUT in an ideal environment devoid of any reflections caused by the ground and the outdoor surroundings. Neither the vector network analyzer, nor the positioner of the indoor far-field chamber were used. Instead our own setup described above was used. Using this RF system gives more realistic reference measurements with which the outdoors measurements can be compared. Four different kinds of measurements were carried out. The first measurement, considered as a reference case, consisted in using the antenna monopole as a probe without the UAS platform. The result is illustrated in red in Figure 5 (bottom). For the second measurement, the antenna probe is mounted on the frame of the UAS when it is turned off. The result, which is illustrated in green in the same figure, shows no impact of the Phantom 3 on the AUT radiation pattern cut. The third measurement, illustrated in blue, represents the AUT radiation pattern cut when the UAS blades are rotating, but when the UAS is not flying. Similarly to the previous case, where the UAS' blades are moving, the AUT radiation pattern cut is not affected. For the fourth measurement, the Phantom 3 was in loitering mode. A Visual Positioning System (VPS) based on ultrasound sensors and camera, in addition to high contrast line grids, were used to keep the UAS stable. The AUT radiation pattern cut,

shown in black in this case, is overlapped with the previous measurements. Discrepancies of about 2 dB were observed. These discrepancies can be attributed to the lack of accuracy of the VPS for indoor application.

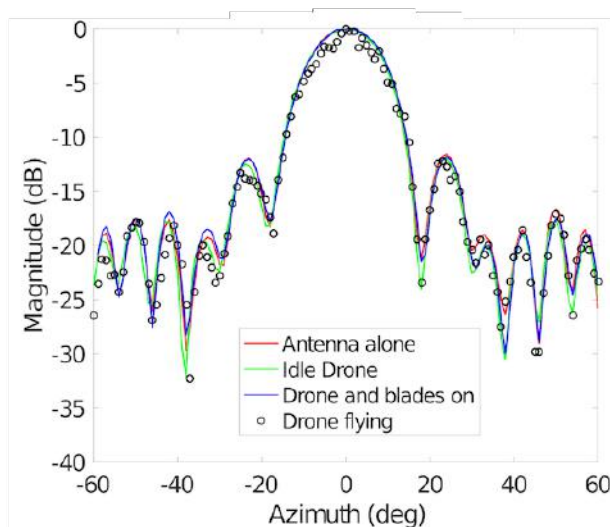
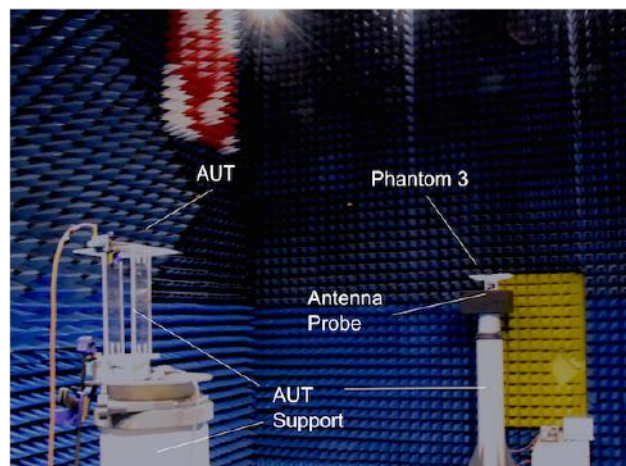


Fig. 5. Indoor antenna pattern cuts measured using the DJI Phantom 3 with a one-quarter-wavelength X-band monopole antenna at the RIL far field anechoic chamber (Dec. 27 2015).

2) *In-situ outdoor measurements:* In this section, the AUT patterns were measured outside at KAEFS (Kessler Atmospheric and Ecological Field Station), an OU facility. The setup considerations are identical to those of the previous section. In this experiment two measurements were performed: a) Measurement of the AUT in scanning mode while the UAS was in loitering mode. b) Measurement of the AUT while the UAS was flying in a circular pattern around it.

The results can be seen in Figures 6 d) and e). The reference pattern cut shown in red was measured with the monopole mounted on a mast. In Figures 6 d), the measured pattern cut when the UAS is loitering is shown. It exhibits discrepancies in the order of 2.7 dB in the main beam, and 3 dB in the sidelobe region. The ripples can be attributed to several factors

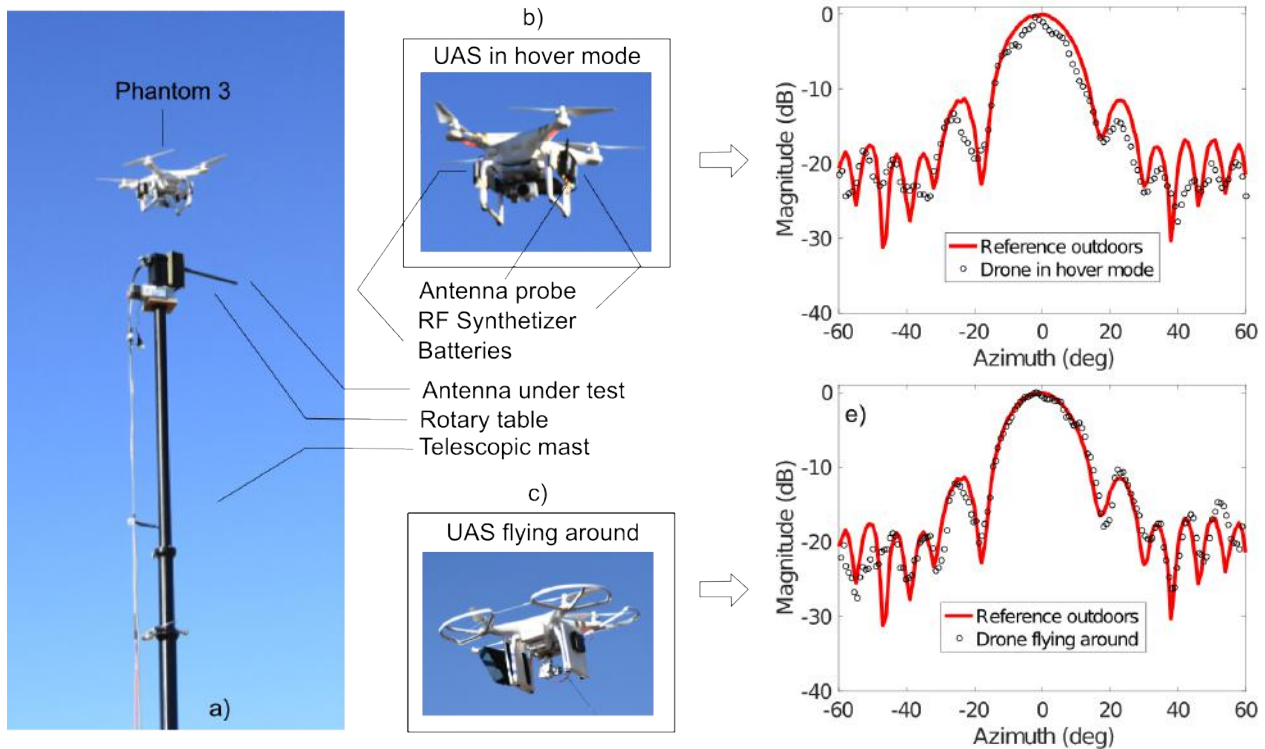


Fig. 6. Outdoor measurements : a) Photograph of the AUT setup at the OU KAEFS facility (Jan. 28 2016). b) Photograph of the small UAS taking the AUT measurements in loiter mode. The AUT is rotating. c) Photograph of the small UAS taking the AUT measurements flying around the AUT (AUT is in a fixed position). d) Measured antenna pattern cut of the AUT using the small UAS in loiter mode. e) Measured antenna pattern cut of the AUT using the small UAS in scanning mode or flying around the AUT.

: the windy conditions (12 mph), the standard GPS accuracy as well as a non-zero roll angle because of payload. In Figure 6 e), the AUT pattern cut when the UAS was flying around is shown. It can be seen that a better agreement was reached because the UAS was more stable in the circular flight pattern than the loitering mode.

#### IV. RADAR CALIBRATION

In this section, a preliminary feasibility study for reflectivity and differential reflectivity based on a UAS is presented for the OU/ARRC X-band RaXPoL radar system. In this case, the UAS carries a foil-wrapped foam sphere of 12 inches. A separation of 20 m between the UAS and the sphere was used in order to distinguish both of their signatures on the radar images. The UAS was operated in loitering mode 35 m above the ground. Using real-time data processing of the RaXPoL, the UAS, as well as the sphere, could be readily located. Once they were found, data was collected in the form of Range Height Indicator (RHI) that can be post-processed. At the same location as for the antenna pattern measurements, the experiment just described was carried out. Twenty-three different  $Z_{dr}$  RHIs could be gathered where the signatures of the UAS and the sphere were distinct. They were filtered according to two criteria. A certain minimum reflectivity threshold, as well as a certain minimum SNR (Signal-to-Noise Ratio) threshold were used to ensure the use of reliable data.

Such an RHI can be seen in Figure 7. Then, over the area where the sphere signature is located,  $Z_{dr}$  was averaged. Once this was done for every single RHI, the standard deviation was computed. For this experiment a value of 0.35 dB for the standard deviation was obtained.

#### V. CONCLUSIONS

A new concept to characterize antenna patterns, inspect radome surfaces, and perform radar calibrations using a UAS platform was presented. A proof of concept using a DJI Phantom 3, with an X-band probe and a foil-wrapped foam sphere, provided preliminary results for antenna characterization and radar calibration. These results confirm that the proposed techniques have potential for future use. The new PAARD UAS platform with new features such as a large payload (a few kilograms), extended flight time (up to 45 minutes), increased stability (adaptive controller), high position accuracy using DGPS and RTK (sub-decimeter) and open-source software, will substantially increase the quality of the results for the proposed missions.

#### ACKNOWLEDGEMENT

The authors would like to thank Kenneth Carson, James Grimsley, Robert Huck, Jeffrey Snyder, and Nafati Aboserwal, for assisting in the flight test at the OU KAEFS facility for the

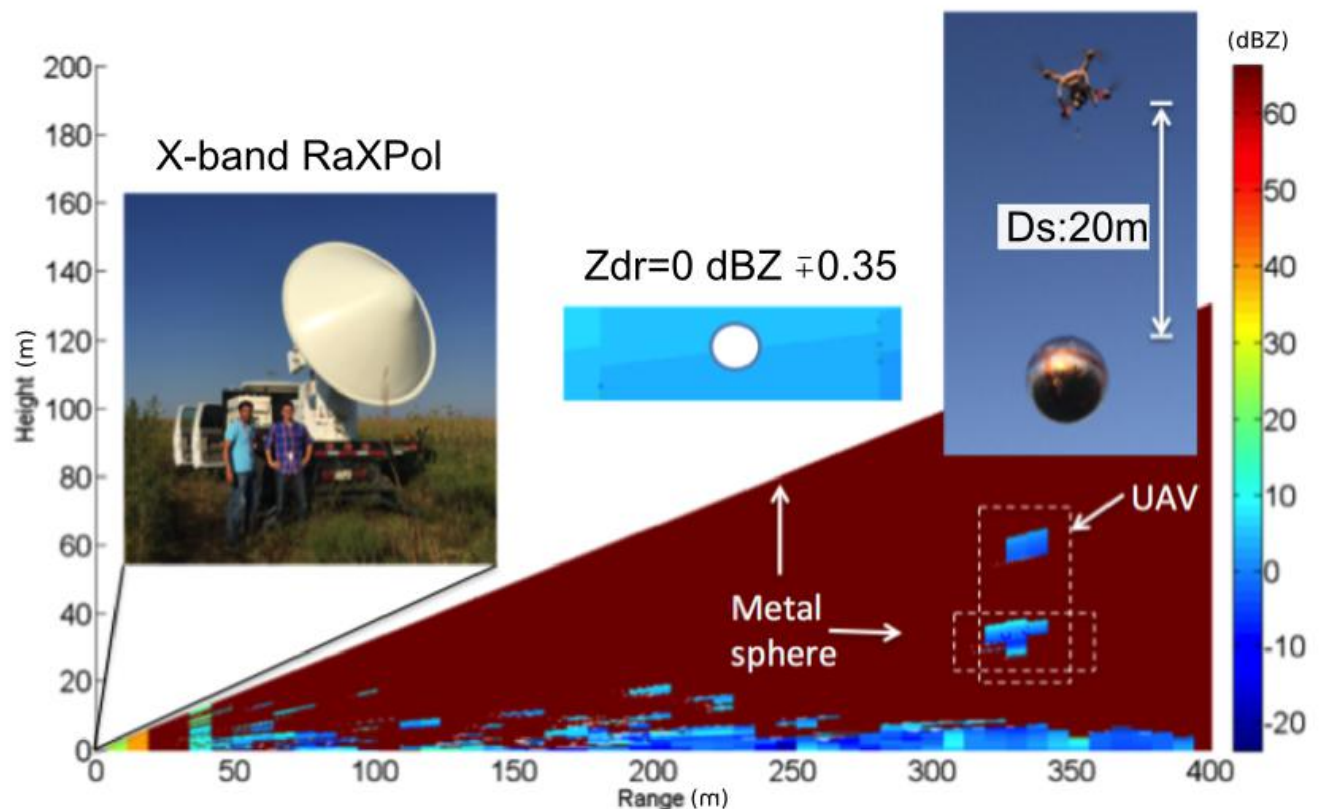


Fig. 7. Radar calibration using the X-band OU/ARRC RaXPol radar system with a suspended 12-inches metal sphere under the UAS (Sept. 23, 2015). This  $Z_{dr}$  RHI shows distinct drone and sphere signatures.

radar calibration test; and Alessio Mancini, Rodrigo Lebron and Brian Brown, for their help in the other measurements.

#### REFERENCES

- [1] R. G. Manton and K. L. Beeke, "Hf antenna radiation patterns over real terrain," in *Broadcasting Convention, 1988. IBC 1988., International*, Sep 1988, pp. 143–147.
- [2] R. J. Doviak, V. Bringi, A. Ryzhkov, A. Zahrai, and D. Zrnic, "Considerations for polarimetric upgrades to operational wsr-88d radars," *Journal of Atmospheric and Oceanic Technology*, vol. 17, no. 3, pp. 257–278, 2000. [Online]. Available: [http://dx.doi.org/10.1175/1520-0426\(2000\)017;0257:CFPUTO;2.0.CO;2](http://dx.doi.org/10.1175/1520-0426(2000)017;0257:CFPUTO;2.0.CO;2)
- [3] Y. Wang and V. Chandrasekar, "Polarization isolation requirements for linear dual-polarization weather radar in simultaneous transmission mode of operation," *IEEE Transactions on Geoscience and Remote Sensing*, vol. 44, no. 8, pp. 2019–2028, Aug 2006.
- [4] J. D. Diaz, J. L. Salazar, J. A. Ortiz, C. Fulton, N. Aboserwal, R. Kelley, and R. Palmer, "A dual-polarized cross-stacked patch antenna with wide-angle and low cross-polarization for fully digital multifunction phased array radars," in *2016 IEEE International Symposium on Phased Array Systems and Technology (PAST)*, Oct 2016, pp. 1–4.
- [5] J. A. Ortiz, J. Daz, N. Aboserwal, J. L. Salazar, L. Jeon, S. Sim, and J. Chun, "Ultra-compact universal polarization x-band unit cell for high-performance active phased array radar," in *2016 IEEE International Symposium on Phased Array Systems and Technology (PAST)*, Oct 2016, pp. 1–5.
- [6] J. L. Salazar, N. Aboserwal, J. D. Daz, J. A. Ortiz, and C. Fulton, "Edge diffractions impact on the cross polarization performance of active phased array antennas," in *2016 IEEE International Symposium on Phased Array Systems and Technology (PAST)*, Oct 2016, pp. 1–5.
- [7] E. R. Williams, K. T. Hood, J. Y. N. Cho, D. J. Smalley, J. B. Sandifer, D. Zrnic, V. M. Melnikov, D. W. Burgess, D. Forsyth, T. M. Webster, and D. Erickson, "End-to-end calibration of nexrad differential reflectivity with metal spheres," *36th Conference on Radar Meteorology (16-20 September, 2013)*, 2013.
- [8] Rieke, "High-precision positioning and real-time data processing of uav systems," in *Conference on Unmanned Aerial vehicle in Geomatics, 2011*, Sep 2011, pp. 1–6.
- [9] F. Üstüner, E. Aydemir, E. Güleç, M. İlerslan, M. Çelebi, and E. Demirel, "Antenna radiation pattern measurement using an unmanned aerial vehicle (uav)," in *General Assembly and Scientific Symposium (URSI GASS), 2014 XXXIth URSI*, Aug 2014, pp. 1–4.
- [10] G. Virone, F. Paonessa, A. Tibaldi, Z. Farooqui, G. Addamo, O. A. Peverini, R. Tascone, P. Bolli, A. Mattana, J. Monari, G. Naldi, F. Perini, G. Pupillo, M. Schiaffino, A. M. Lingua, M. Piras, P. Maschio, I. Aicardi, I. H. Bendea, and A. Cina, "Uav-based radiation pattern verification for a small low-frequency array," in *2014 IEEE Antennas and Propagation Society International Symposium (APSURSI)*, July 2014, pp. 995–996.
- [11] G. Virone, F. Paonessa, O. A. Peverini, G. Addamo, R. Orta, R. Tascone, and P. Bolli, "Antenna pattern measurements with a flying far-field source (hexacopter)," in *Antenna Measurements Applications (CAMA), 2014 IEEE Conference on*, Nov 2014, pp. 1–2.
- [12] G. Virone, A. M. Lingua, M. Piras, A. Cina, F. Perini, J. Monari, F. Paonessa, O. A. Peverini, G. Addamo, and R. Tascone, "Antenna pattern verification system based on a micro unmanned aerial vehicle (uav)," *IEEE Antennas and Wireless Propagation Letters*, vol. 13, pp. 169–172, 2014.
- [13] F. Paonessa, G. Virone, I. Aicardi, A. M. Lingua, M. Piras, P. Maschio, P. Bolli, G. Addamo, O. A. Peverini, R. Orta, and R. Tascone, "Recent results in antenna pattern measurement with uavs," in *Electromagnetics in Advanced Applications (ICEAA), 2015 International Conference on*, Sept 2015, pp. 720–721.